



Electronic Materials

DOW ELECTRONIC MATERIALS

INTERCONNECT TECHNOLOGIES

Interpretation of texture changes during self-annealing of electroplated copper

The article is published at Microelectronic Engineering, Dec. 2010

W.Q. Zhang, A.D. Li , K.B. Yin, Y.D. Xia, Z.G. Liu

National Laboratory of Solid State Microstructures, Department of Materials Science and Engineering, Nanjing University, Nanjing 210093, PR China

G.B. Ma

National Laboratory of Solid State Microstructures, Department of Physics, Nanjing University, Nanjing 210093, PR China

C.Y. Chan , K.L. Cheung , M.W. Bayes , K.W. Yee

Dow Electronic Materials, The Dow Chemical Company, 15 On Lok Mun St., On Lok Tsuen, Fanling, Hong Kong, PR China

Abstract

Electroplating of copper is widely used for the fabrication of interconnections of printed circuit boards, in which via-holes are used to connect conductive layers. Self-annealing is an important feature of electroplated copper which significantly alters its microstructures. The degradation of $\langle 1\ 1\ 0 \rangle$ texture and the enhancement of $\langle 3\ 1\ 1 \rangle$ texture in electroplated copper during self-annealing process are observed by X-ray diffraction (XRD) and electron backscattering diffraction (EBSD). The mechanism of this transformation is discussed and illustrated.

Keywords:

Self-annealing, Electroplated copper, Texture evolution, X-ray diffraction (XRD), Electron backscattering diffraction (EBSD)

Introduction

Recently, increased demands for miniaturization and efficiency of electronic devices have made build-up processes a key technology for the fabrication of printed circuit boards (PCBs), in which via-holes are used to connect conductive layers. Both the interlayer connection and the filling of via-holes are accomplished by copper electroplating [1].

Copper electroplating is widely used for the fabrication of interconnections of PCBs, for systems-in-package, and semiconductor devices [2]. Electrodeposition of copper has a long tradition, and many decades ago it was observed that the microstructure of copper changes as a function of time. Since the era of copper interconnects, this so called self-annealing effect has been studied in more detail. There is no doubt that self-annealing has a substantial effect on the microstructure and the associated physical properties of electroplated copper. Experimental observations of decreasing electrical resistivity and hardness, improving ductility, and increasing grain size and surface roughness, as well as changes in crystallographic texture and the level of internal stresses as a function of time at room temperature are frequently reported [3–12]. It is generally reported that in electroplated copper films, degradation of $\langle 1\ 1\ 1 \rangle$ texture is observed during self-annealing process [6,11,13]. Ueno *et al.* reported that $\langle 1\ 1\ 1 \rangle$ texture of electroplated copper films deposited on $\langle 1\ 1\ 1 \rangle$ textured seed layers decreased during self-annealing [14], while it is reported by Surnev *et al.* that the type of recrystallization texture depends on the growth texture preparation conditions [15].

In this work, we observe the degradation of $\langle 1\ 1\ 0 \rangle$ texture and the enhancement of $\langle 3\ 1\ 1 \rangle$ texture in electroplated copper during self-annealing process. This transformation, which is deviating from the ones commonly observed [16,17], and its mechanism are discussed and illustrated.

Microstructures of electroplated copper are analyzed using electron backscattering diffraction (EBSD) to obtain orientation maps, pole figures and inverse pole figures. X-ray diffraction (XRD) measurements are used to provide crystallographic information.

Experimental

PCBs with resin and glass fiber interspaced, and about several micron-thick polycrystalline copper on both surfaces were used as the substrates for sample preparation. The plating bath, agitated by air bubbles, consisted of a mixture of sulfuric acid, copper sulfate, hydrochloric acid, water, and proprietary additives. The plating was done at room temperature (approximately 25 °C). Direct current was used in this study, at a current density of 0.75 A/dm². The thickness of the plated copper foils was about 15 μm. The copper anode contained a small percentage of phosphorus. To accelerate the self-annealing rate, some samples were annealed at 120 °C for 4 h, and then dipped into sulfuric acid solution (5% by volume) to remove surface oxidation. The samples were characterized in plain-view.

EBSD is a scanning electron microscopy (SEM) based technique. Diffracted backscattered electrons form a pattern on a phosphor screen, which is placed inside the SEM chamber. Diffraction patterns are then processed in order to obtain orientation maps, pole figures, grain size information, etc. EBSD is a relatively fast, highly sensitive and local electron diffraction analysis that can be performed over large areas [18–21].

The EBSD system used in this study is attached to a high resolution field emission gun SEM instrument (Leo 1530-VP FEG-SEM). The measurements were carried out at a working distance of 14 mm and an accelerating voltage of 21 kV. The diameter of the aperture was 120 μm . The software used for the data acquisition and the subsequent analysis of the EBSD measurements were EDAX-TSL OIM Data Collection 3.5 and EDAX-TSL OIM Analysis 3.0, respectively [22–24].

In EBSD measurements, areas of 40 x 40 μm^2 were scanned at a step interval of 0.3 μm . The data from these scans are presented in three separate formats: an orientation image, pole figures and inverse pole figures, which are recorded for the copper foils which have been self-annealed for 96 days at room temperature after electrodeposition and then annealed at 120 °C for 4 h.

Structures and orientations of electroplated copper on the surface of PCB substrates were characterized in plain-view by XRD using a D/Max-rA diffractometer (Rigaku, Japan) with Cu K α radiation. The measurement was performed in Bragg Brentano geometry ($\theta/2\theta$ geometry) operating at the power of 40 kV 100 mA with the beam size of 0.5 mm x 10 mm. The 2 h scan range was from 40° to 93° with a step size of 0.02° and a preset time of 0.2 s. Data were fit using Jade 5.0 software (Materials Data, Inc.) with Pearson VII curve profile function.

Crystallite size was deduced from the Scherrer formula $\langle D \rangle = K\lambda / \beta_{1/2} \cos \theta$ [25], in which $\beta_{1/2}$ was the corrected peak broadening (full width half maximum, FWHM) expressed in radian, λ was the X-ray wavelength ($\lambda = 1.5406$ Å), θ was the incident Bragg angle, $\langle D \rangle$ was the average volume crystal size, and K was the crystallite shape factor. Assuming that the crystallite is spherical with cubic symmetry, the value of K constant is approximately 0.9 [26].

Results

Fig. 1(a) shows the XRD pattern characterizing the polycrystalline copper of PCB substrate used in our study. The four peaks are assigned to (1 1 1), (2 0 0), (2 2 0), and (3 1 1), which all match standard data from polycrystalline copper powders (JCPDS 040836, Fig. 1(b)) [27]. In order to evaluate the copper grain orientations of the PCB substrate, we made a comparison of XRD data between the substrate and standard polycrystalline copper powders (JCPDS 04-0836), as listed in Table 1.

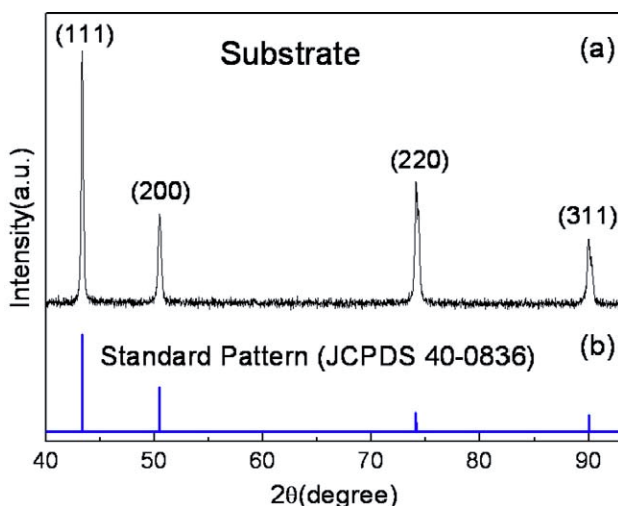


Fig. 1. XRD patterns for (a) polycrystalline copper of PCB substrate and (b) standard polycrystalline copper powders (JCPDS 40-0836).

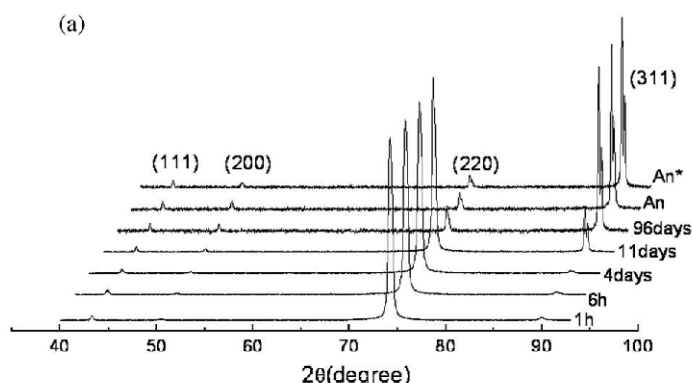
In the XRD pattern of standard polycrystalline copper powders, the four peaks are (1 1 1), (2 0 0), (2 2 0), and (3 1 1), whose relative peak intensities (RPI) to the highest peak (1 1 1) are 100%, 46%, 20% and 17%, respectively, as shown in Table 1. For the poly-crystalline copper of PCB substrate, RPI of the four peaks are 100%, 36.6%, 54.7% and 27.6%, respectively. In order to have a direct comparison of the data without referring to the fractions of standard polycrystalline copper powders, all the data presented below have been normalized and presented as NPI (normalized peak intensity), which are calculated as follows (using XRD pattern of PCB substrate for example): RPI of the corresponding four peaks are compared between the PCB substrate and standard polycrystalline copper powders, and the quotient values are then normalized with the sum as 1 to obtain NPI of the PCB substrate. It should be emphasized that all the XRD patterns are quantified using NPI mentioned above throughout the manuscript.

It is obvious that, from the data listed in Table 1, NPI of standard polycrystalline copper powders are 0.25 for each peak, and NPI of the PCB substrate are quite different from this standard value. In detail, NPI of (1 1 1) and (2 0 0) peaks are 0.16 and 0.13, respectively, which are smaller than 0.25. For (3 1 1) peak, NPI is 0.26, similar to 0.25. However, NPI of (2 2 0) peak is 0.45, much larger than 0.25, indicating that $\langle 1\ 1\ 0 \rangle$ orientation is relatively strong for the PCB substrate, which may influence the following electrodeposition process.

Table 1. RPI and NPI of XRD patterns for standard polycrystalline copper powders and copper surface of the PCB substrate. (RPI-relative peak intensities to the highest peak, NPI normalized peak intensities).

	Peaks	(1 1 1)	(2 0 0)	(2 2 0)	(3 1 1)
Standard polycrystalline copper powders	RPI	100%	46%	20%	17%
	NPI	0.25	0.25	0.25	0.25
Copper surface of PCB substrate	RPI	100%	36.6%	54.7%	27.6%
	NPI	0.16	0.13	0.45	0.26

XRD profiles (Fig. 2(a-c)) of copper foils (electroplated at a current density of 0.75 A/dm² obtained at different stages of self-annealing, show significant changes in the crystallographic orientations of the copper foils over time. The as-deposited foils were predominantly $\langle 110 \rangle$ oriented, probably influenced by the orientations of the substrate and several other factors, such as current densities and bath additive contents [16,28]. The intensity of (2 2 0) peak began to decrease rapidly between the 4th and 11th days after deposition. Meanwhile, (3 1 1) peak began to increase after the 4th day after deposition, and finally became the dominant orientation, replacing (2 2 0) peak, after the 96th day. During this period, the intensities of the other two peaks (1 1 1) and (2 0 0) did not show noticeable changes. For comparison, the as-deposited sample was annealed at 120 °C for 4 h, assigned as “An”, while the sample stored at room temperature (RT) for 96 days after deposition was also annealed using the same method, assigned as “An*”. As shown in Fig. 2(a), the crystallographic orientations of these two annealed samples were almost the same as that of the sample stored at RT for 96 days after deposition. This indicates that the room temperature self-annealing process had slowed down to a relatively stable state at this point, with a predominance of $\langle 3\ 1\ 1 \rangle$ orientation.



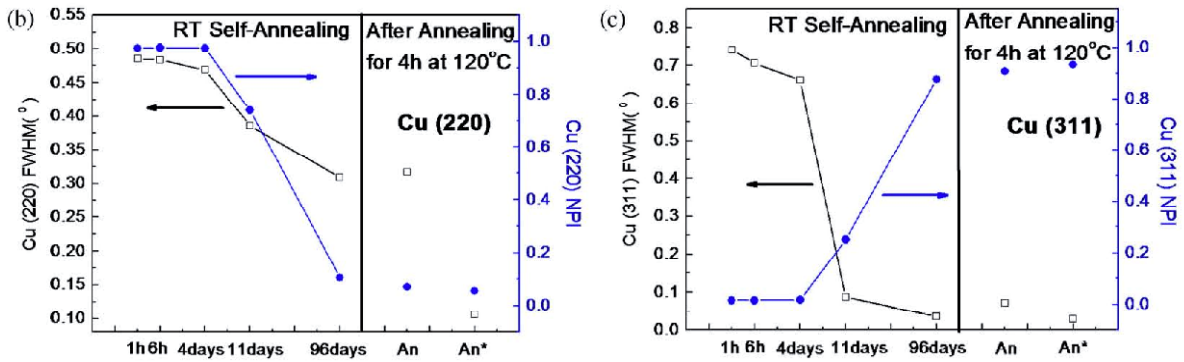


Fig.2. (a) XRD profiles at different stages of self-annealing, and dependence of FWHM and NPI of (b) (2 2 0) and (c) (3 1 1) peaks on time. “An” refers to electroplated copper foils annealed at 120 °C for 4 h immediately after deposition, and “An*” refers to the foils annealed at 120 °C for 4 h after 96 days storage at room temperature after deposition.

Fig. 2(b) and (c) reveal the evolution of FWHM and NPI of (2 2 0) and (3 1 1) line profiles versus time. During self-annealing, both (2 2 0) and (3 1 1) peaks became narrower, but at different rates. The FWHM of (2 2 0) peak changed from 0.48° to 0.32° while (3 1 1) peak underwent a steeper drop from 0.74° to 0.03°. Concerning to NPI, it is obvious that, in the as-deposited state, (3 1 1) peak was much weaker than (2 2 0). Over the first four days, the NPI of (2 2 0) and (3 1 1) peaks remained constant. Starting from this point, both peak intensities changed rapidly, with a decrease of (2 2 0) NPI and an increase of (3 1 1) NPI. This indicates that the volume fraction of <1 1 0> orientation decreased substantially, while that of <3 1 1> orientation showed a corresponding increase during the course of self-annealing. In EBSD measurement, to assign orientations, color contours are used for both pole figures and inverse pole figures to show the strength of the texture compared to a random texture. Different colors stand for different relative strengths as shown in the color legend on the right side.

The EBSD orientation image shown in Fig. 3(a) can be interpreted as follows. Grains marked pink are oriented with {3 1 1} planes parallel to the sample surface, while grains in red, green and blue have {1 0 0}, {1 0 1} and {1 1 1} planes parallel to the sample surface, respectively. Fig. 3(b) provides a color legend to interpret this image. Most of the grains shown in Fig. 3(a) are pink.

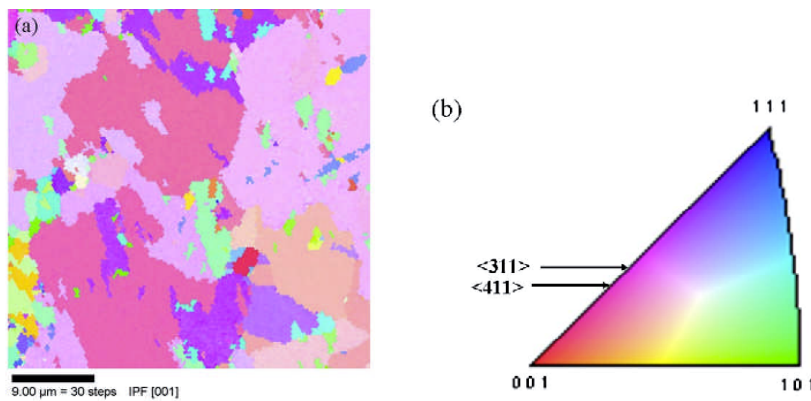


Fig.3. (a) EBSD orientation maps of electroplated copper foils annealed for 4 h at 120 °C after storage at room temperature for 96 days.(b) The orientation color key.

Fig. 4(a) shows {2 0 0}, {2 2 0}, {3 1 1} and {1 1 1} pole figures for the annealed copper foils. Rolling direction (RD) and transverse direction (TD) are reference directions in the observed sample plane. For comparison, theoretic pole figures of the standard <3 1 1> single crystal copper are shown in Fig. 4(b), in which red points represent symmetrically equivalent planes in the crystal. Most of the red areas with the highest strength in Fig. 4(a) correspond to those red points in Fig. 4(b), which indicates that <3 1 1> grains are dominant, although the sample is polycrystalline copper.

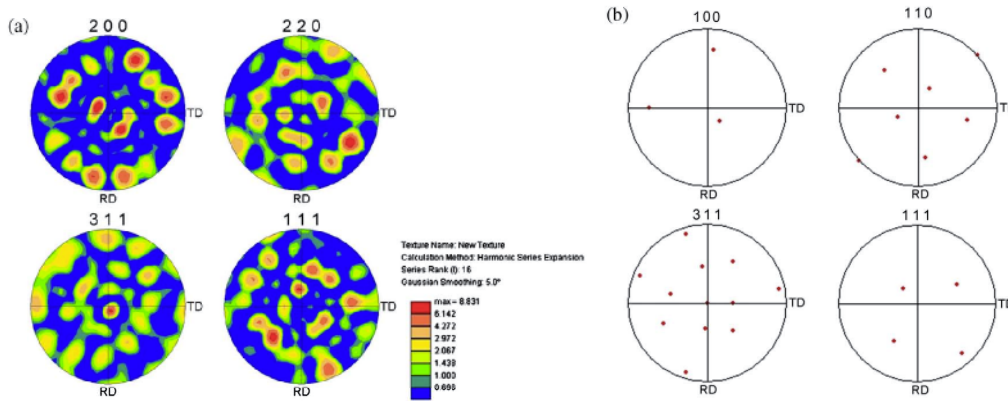


Fig.4.(a) {2 0 0}, {2 2 0}, {3 1 1} and {1 1 1} pole figures for electroplated copper foils annealed for 4 h at 120 °C after storage at room temperature for 96 days.(b)Theoretic pole figures of the standard <311> single crystal copper.

The red area in the inverse pole figure at normal direction (see Fig. 5(a)) is concentrated at the range around the point standing for <3 1 1> orientation, verifying the results obtained from pole figures. The data shown in Figs. 4(a) and 5(a) are therefore consistent with the presence of predominant <3 1 1> orientation.

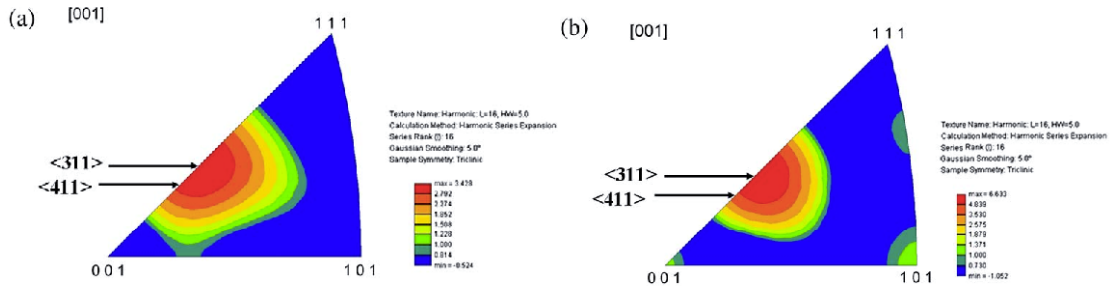


Fig. 5. Inverse pole figures for electroplated copper foils annealed for 4 h at 120 °C after storage at room temperature for (a) 96 days and (b) 700 days.

Based on the above analysis, <3 1 1> is probably the predominant orientation for this annealed copper foil, with a typical grain size of several micrometers in diameter (in Fig. 3(a)), which is confirmed by focused ion beam (FIB) images obtained from the same sample. The process of self-annealing might involve recovery, recrystallization, and/or grain growth [3]. The changes in the process of self-annealing for electroplated copper foils can be visualized as follows. A combination of three factors: (i) the proprietary additives incorporated in the electroplating solution, (ii) the electroplating conditions and (iii) a substrate with relatively strong <1 1 0> orientation, led to the formation of a deposit in which the majority of grains were <1 1 0> oriented in the as-deposited copper foils, although there were small proportion of other grains such as <1 1 1>, <1 0 0> and <3 1 1>. The grain size in this stage is very small and can be evaluated according to Scherrer equation using FWHM of (2 2 0) peak. It was estimated as about twenty nanometers in diameter. During the initial period after deposition (1 h to 4 days), XRD patterns show a consistent crystallographic texture, implying that recrystallization accompanied by dramatic texture changes did not occur initially. It is observed that, in Fig. 2(b) and (c), FWHMs for (2 2 0) and (3 1 1) in this stage keep almost constant, about 0.47° and 0.7°, respectively, meanwhile NPI for the two peaks maintain about 0.95 and 0.01, respectively. This stage has been referred to as “recovery”, an incubation time before the onset of recrystallization and grain growth. During this stage, the microstructure is not stable, as indicated by the slightly decreasing diffraction linewidth [3]. Detavernier *et al.* [12] illustrated that the recovery process consists of the annihilation of point defects and dislocations produced during deposition and the spontaneous rearrangement of dislocations into low-angle subgrain boundaries.

During the next stage (4 days to 96 days), sudden and strong changes of XRD intensities (Fig. 2(a–c)) indicate the transformation of the microstructure induced by recrystallization and/or grain growth. The marked changes in this stage are the rapid increase of (3 1 1) peak intensity and decrease of (2 2 0) peak intensity, accompanied by grain growth, reflected by FWHM narrowing. As shown in Fig. 2, on the 11th day, (3 1 1) peak intensity increased, with NPI of 0.25, while (2 2 0) peak had no obvious change with NPI of 0.74. On the 96th day, (3 1 1) peak was much higher, while (2 2 0) peak was much lower, and their NPI were 0.88 and 0.11, respectively. During this period, FWHM of (2 2 0) peak changed from 0.47° to 0.31° and that of (3 1 1) underwent a steeper drop from 0.66° to 0.04° .

Finally, the electroplated copper foils stored at room temperature for 96 days reached a relatively stable stage without distinguish further changes

Discussion

Having observed the important differences between textures of electroplated copper foils as-deposited and after self-annealing, the question arises as how the new orientations are formed within the highly oriented matrix of the fine-grained copper. Both Pantleon et al. [3,13] and Lingk et al. [6] reported that copper, having low stacking fault energy, can easily undergo multiple twinning in the early stages of a growth process, which may be the leading mechanism for the texture transformation during self-annealing. Berger et al. [29] describe a three step process: (1) nucleation of new grains, (2) twinning in early stages, and (3) subsequent growth, providing a way to understand the emergence of new orientations.

Merchant et al. [30] also suggest that twinning is the most likely means of preferential grain growth in the direction of twinning planes, which for the face-centered cubic metals, such as copper, are {1 1 1} planes. It is well known that twinning of $\langle 1\ 1\ 0 \rangle$ results in $\langle 4\ 1\ 1 \rangle$ [30]. Therefore, according to [6] and [29], the first order twinning of the parent orientation as $\langle 1\ 1\ 0 \rangle$ is $\langle 4\ 1\ 1 \rangle$. A calculation of the pole figure for $\langle 1\ 1\ 0 \rangle$ orientation with the presence of {1 1 1} twinning planes, shows five dots in the pole figure (illustrated in Fig. 6(a)), of which two are on both sides of the center in the figure, 35° away, and the other three ones are on the circle, 90° to the center. The pole figure of the corresponding fiber texture for this orientation is shown in Fig. 6(b), in which the two dots form a ring at 35° and the other three dots form a ring at 90° with the same center. The same analysis for $\langle 4\ 1\ 1 \rangle$ orientation, gives three rings at 35° , 57° and 74° with the same center [31], as shown in Fig. 6(c) and (d). For fiber textures, peaks appear as rings in the pole figures, indicating that the material has no preferred in-plane orientation. Superposition of the rings and dots for $\langle 1\ 1\ 0 \rangle$ and $\langle 4\ 1\ 1 \rangle$ orientations as shown in Fig. 6(e) reveals that the angular separation between {1 1 1} and {1 1 0} crystal planes and that between {1 1 1} and {4 1 1} crystal planes are the same, which means {1 1 0} and {4 1 1} planes are twinning with {1 1 1} twinning plane. As described in [30], twinning of $\langle 1\ 1\ 1 \rangle$ results in $\langle 5\ 1\ 1 \rangle$ and the twinning of $\langle 100 \rangle$ in $\langle 2\ 2\ 1 \rangle$. These phenomena can also be explained by the similar approach described above, which proves that another orientation can be generated by the first order twinning from a parent orientation.

On the other hand, surface/interface energy may strongly influence the microstructure evolution through control of texture [5]. The surface energies of various crystal planes were calculated by Zhang et al. [32]. The surface energies of {3 1 1} and {4 1 1} crystal planes were calculated to be 1.645 J/m^2 and 1.675 J/m^2 , respectively. It is obvious that the surface energy of {3 1 1} is somewhat smaller than that of {4 1 1}. The angular separations between {3 1 1} and {4 1 1} crystal planes may be calculated to be 6° , 32° , 45° , 55° , 65° , 82° and 90° . Thus, {4 1 1} crystal planes need only tilt about 6° , in order to transform into {3 1 1} to reduce the surface smaller than that of {4 1 1}.

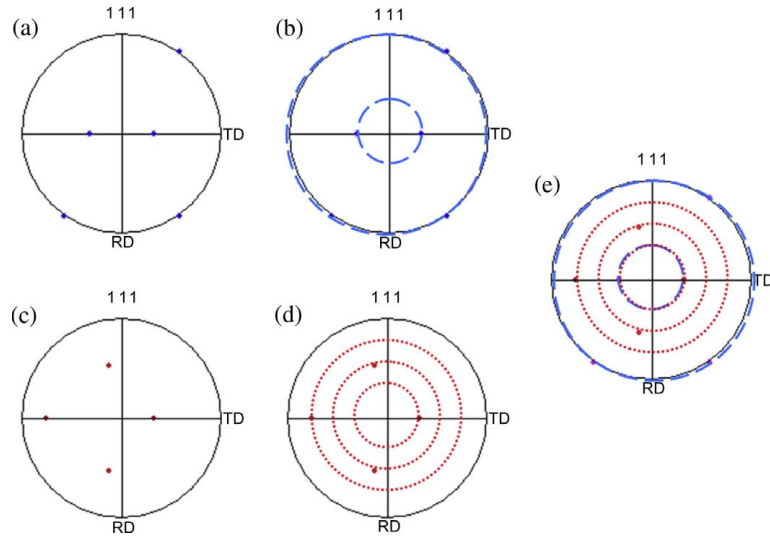


Fig. 6. (a) $\{1\ 1\ 1\}$ Pole figure for a $\langle 1\ 1\ 0 \rangle$ -oriented crystal; (b) pole figure for a film with $\langle 1\ 1\ 0 \rangle$ fiber texture; (c) $\{1\ 1\ 1\}$ pole figure for a $\langle 4\ 1\ 1 \rangle$ -oriented crystal; (d) $\{1\ 1\ 1\}$ pole figure for a film with $\langle 4\ 1\ 1 \rangle$ fiber texture; (e) superposition of pole figures for $\langle 1\ 1\ 0 \rangle$ and $\langle 4\ 1\ 1 \rangle$ textures.

Therefore, the texture transformation from $\langle 1\ 1\ 0 \rangle$ to $\langle 3\ 1\ 1 \rangle$ can be explained that $\langle 1\ 1\ 0 \rangle$ orientation firstly underwent a first order twinning to $\langle 4\ 1\ 1 \rangle$, then followed by a tilt of about 6° to reach $\langle 3\ 1\ 1 \rangle$, driven by a reduction in surface energy.

Furthermore, in the inverse pole figure (as shown in Fig. 5(a)), the points standing for $\langle 3\ 1\ 1 \rangle$ and $\langle 4\ 1\ 1 \rangle$ orientations are quite close to each other and the red area showing maximum strength is broad and covers both points, which may indicate a co-existence of $\langle 3\ 1\ 1 \rangle$ and $\langle 4\ 1\ 1 \rangle$ grains after self-annealing. Moreover, another inverse pole figure (Fig. 5(b)), showing narrower maximum toward $\langle 3\ 1\ 1 \rangle$, was obtained from the copper foils electroplated in the same condition above, then annealed at 120°C for 4 h after storage at room temperature for 700 days. It can be observed that, in Fig. 5(a), both $\langle 3\ 1\ 1 \rangle$ and $\langle 4\ 1\ 1 \rangle$ points belong to the same red area, unable to be distinguished, indicating similar strengths, and the strengths of the texture compared to a random texture are 3.41 and 3.10 respectively. However, in Fig. 5(b), $\langle 3\ 1\ 1 \rangle$ and $\langle 4\ 1\ 1 \rangle$ points belong to different color contours, and they can be separated easily. Referred to the color legend, the relative strengths of both orientations are growing, and their values are 6.61 and 5.06, respectively. Growth of relative strengths indicate that more $\langle 3\ 1\ 1 \rangle$ and $\langle 4\ 1\ 1 \rangle$ grains are formed, and larger difference between the two orientations shows transformation from $\langle 4\ 1\ 1 \rangle$ to $\langle 3\ 1\ 1 \rangle$ orientation. Therefore, $\langle 4\ 1\ 1 \rangle$ grains will slowly transform to $\langle 3\ 1\ 1 \rangle$ finally after enough long time.

The following grain growth consists of an increase of the mean radius of the nucleated grains. The driving force in this case is the minimization of total grain boundary energy in the system with the effect of the proprietary additives incorporated in the electroplating solution [12,33].

Conclusion

In this paper, the degradation of $\langle 1\ 1\ 0 \rangle$ texture and enhancement of $\langle 3\ 1\ 1 \rangle$ texture in electroplated copper during self-annealing are characterized using XRD and EBSD. The pathway for textural transformation is attributed to the first order twinning in the early stages of the growth process, with $\langle 1\ 1\ 0 \rangle$ orientation undergoing twinning to $\langle 4\ 1\ 1 \rangle$, followed by slow evolution to $\langle 3\ 1\ 1 \rangle$ to reduce the surface energy. The driving force for the following grain growth is the minimization of total grain boundary energy in the system.

Acknowledgements

This project was supported by Dow Electronic Materials, the Dow Chemical Company, as well as the Natural Science Foundation of China (50672036 and 10974085) and a grant from the State Key Program of China (2009ZX02101-004 and 2009CB929500). Aidong Li also thank the support from the program for the "333" Talents in Jiangsu Province and SRF for ROCS, SEM.

References:

- [1] S. Miura, H. Honma, *Surf. Coat. Tech.* 169–170 (2003) 91–95.
- [2] M. Hasegawa, Y. Nonaka, Y. Negishi, Y. Okinaka, T. Osaka, *J. Electrochem. Soc.* 153 (2) (2006) C117–C120.
- [3] K. Pantleon, M.A.J. Somers, *J. Appl. Phys.* 100 (2006) 114319.
- [4] C. Lingk, M.E. Gross, *J. Appl. Phys.* 84 (10) (1998) 5547.
- [5] J.M.E. Harper, C. Cabral Jr., P.C. Andricacos, L. Gignac, I.C. Noyan, K.P. Rodbell, C.K. Hu, *J. Appl. Phys.* 86 (5) (1999) 2516.
- [6] C. Lingk, M.E. Gross, W.L. Brown, *J. Appl. Phys.* 87 (5) (2000) 2232.
- [7] S.P. Hau-Riege, C.V. Thompson, *Appl. Phys. Lett.* 76 (3) (2000) 309.
- [8] S.C. Chang, J.M. Shieh, B.T. Dai, M.S. Feng, *J. Electrochem. Soc.* 149 (9) (2002) G535–G538.
- [9] V.A. Vasko, I. Tabakovic, S.C. Riemer, *Electrochem. Solid State Lett.* 6 (7) (2003) C100–C102.
- [10] C. Detavernier, D. Deduytsche, R.L.V. Meirhaeghe, J.D. Baerdemaeker, C. Dauwe, *Appl. Phys. Lett.* 82 (12) (2003) 1863.
- [11] H. Lee, S.S. Wong, S.D. Lopatin, *J. Appl. Phys.* 93 (7) (2003) 3796.
- [12] C. Detavernier, S. Rosnagel, C. Noyan, S. Guha, C. Cabral Jr., C. Lavoie, *J. Appl. Phys.* 94 (5) (2003) 2874.
- [13] K. Pantleon, M.A.J. Somers, *Scripta Mater.* 55 (2006) 283–286.
- [14] K. Ueno, T. Ritzdorf, S. Grace, *J. Appl. Phys.* 86 (9) (1999) 4930.
- [15] Sv. Surnev, I. Tomov, *J. Appl. Electrochem.* 19 (1989) 752–757.
- [16] M. Stangl, M. Liptak, A. Fletcher, J. Acker, J. Thomas, H. Wendrock, S. Oswald, K. Wetzig, *Microelectr. Eng.* 85 (2008) 534–541.
- [17] V.A. Vas'ko, I. Tabakovic, S.C. Riemer, M.T. Kief, *Microelectr. Eng.* 75 (2004) 71–77.
- [18] S. Courtasa, M. Grégoireb, X. Federspiela, N. Bicaïs-Lepinayb, C. Wyonc, *Microelectron. Reliab.* 46 (2006) 1530–1535.
- [19] U.S. Chen, H.C. Shih, *Nucl. Instrum. Meth. B* 237 (2005) 477–483.
- [20] A.J. Wilkinson, P.B. Hirsch, *Micron* 28 (4) (1997) 279–308.
- [21] D.T. Read, Y.W. Cheng, R. Geiss, *Microelectr. Eng.* 75 (2004) 63–70.
- [22] J.D. Kang, X.H. Hu, S.I. Wright, P.D. Wu, D.S. Wilkinson, R.K. Mishra, *Metall. Mater. Trans. A* 39A (2008) 2007–2013.
- [23] S. Zaefner, S.I. Wright, D. Raabe, *Metall. Mater. Trans. A* 39A (2008) 374–389.
- [24] Y. Zhao, H.L. Suo, Y.H. Zhu, J.-C. Grivel, M.M. Gao, L. Ma, R.F. Fan, M. Liu, Y. Ji, M.L. Zhou, *Acta Mater.* 57 (2009) 773–781.
- [25] P. Scherrer, *Nachr. Ges. Wiss. Göttingen* 26 (1918) 98–100.
- [26] A.L. Patterson, *Phys. Rev.* 56 (1939) 978–982.
- [27] H.E. Swanson, E. Tatge, *Natl. Bur. Stand. (US), Circ.* 539 (1953) I, 15.
- [28] A.A. Rasmussen, J.A.D. Jensen, A. Horsewell, M.A.J. Somers, *Electrochim. Acta* 47 (2001) 67–74.
- [29] A. Berger, P.J. Wilbrandt, F. Ernst, U. Klement, P. Haasen, *Prog. Mater. Sci.* 32 (1988) 1–95.
- [30] H.D. Merchant, O.B. Girin, *Mater. Res. Soc. Proc.* 431 (1997) 433–444.
- [31] M.T. Pérez-Prado, J.J. Vlassak, *Scripta Mater.* 47 (2002) 817–823.
- [32] J.M. Zhang, F. Ma, K.W. Xu, *Appl. Surf. Sci.* 229 (2004) 34–42.
- [33] H. Lee, W.D. Nix, S.S. Wong, *J. Vac. Sci. Technol. B* 22 (5) (2004) 2369–2374.